Frontiers of Information Technology & Electronic Engineering
www.jzus.zju.edu.cn; engineering.cae.cn; www.springerlink.com
ISSN 2095-9184 (print); ISSN 2095-9230 (online)
E-mail: jzus@zju.edu.cn

Deceptive jamming discrimination based on range-angle localization of a frequency diverse array

Zhao-jian ZHANG[†‡], Jun-wei XIE, Chuan SHENG, Zhun TANG
(*Air and Missile Defense College, Air Force Engineering University, Xi'an 710051, China*)
[†]E-mail: zzj554038@163.com

Received Sept. 22, 2016; Revision accepted Jan. 4, 2017; Crosschecked Sept. 30, 2017

Abstract: We propose a method to suppress deceptive jamming by frequency diverse array (FDA) in radar electronic countermeasure environments. FDA offers a new range-angle-dependent beam pattern through a small frequency increment across elements. Due to the coupling between the angle and range, a mismatch between the test angle and physical angle occurs when the slant range on which the beam focuses is not equal to the slant range of the real target. In addition, the range of the target can be extracted by sum-difference beam except for time-delay testing, because the beam provides a range resolution in the FDA that cannot be deceived by traditional deceptive jamming. A strategy of using FDA to transmit two pulses with zero and nonzero frequency increments, respectively, is proposed to ensure that the angle of a target can be obtained by FDA. Moreover, the localization performance is examined by analyzing the Cramer-Rao lower bound and detection probability. Effectiveness of the proposed method is confirmed by simulation results.

Key words: Frequency diverse array (FDA); Deceptive jamming; Range-angle coupling; Sum-difference beam; Double-pulse
https://doi.org/10.1631/FITEE.1601577 **CLC number:** TN974

1 Introduction

In electronic countermeasure (ECM) environments, the transmitted pulse from radar can be easily picked up and retransmitted by a jammer. By amplifying the repeated signal, the repeat jammer may produce a series of false targets (FTGs), which can be overlapped with echo in both time and frequency domains. FTGs are in the main beam and are highly correlated with the real target (RTG); thus, radar cannot easily identify and suppress them. Several strategies have been proposed to combat deception jamming over the last several decades. Parameter agility during the pulse has been studied (Akhtar, 2009; Lu *et al*., 2011; 2013; 2016; Zhang *et al*., 2013; Xiong *et al*., 2016) and random orthogonal frequency division multiplexing (OFDM) signals (Schuerger and Garmatyuk, 2009) have been adopted, which can create more difficulties for the jammer in intercepting the radar's waveform. However, if the jammer is powerful enough to follow the radar and is able to retransmit the signal within one pulse repetition period, FTGs can be generated effectively as well. Other strategies focus on the analysis of signal features, such as polarization (Huang *et al*., 2013), fluctuation characteristics (Rao *et al*., 2010), and correlation (Rao *et al*., 2011; Zhao *et al*., 2015), the aim of which is to distinguish the true target from FTGs based on signal feature differences. These methods have high computational costs and the information needed can be hard to extract.

Frequency diverse array (FDA), which can generate a range-angle-dependent beam pattern through a small frequency increment across the elements, was first proposed by Antonik *et al*. (2006). Because of its potential applications in signal processing, FDA has attracted substantial attention in recent years. The characteristics of the FDA beam

[‡] Corresponding author
ORCID: Zhao-jian ZHANG, http://orcid.org/0000-0003-3703-0314

pattern have been analyzed (Cullens *et al*., 2012), and the design strategies of the FDA radar system and receiver architectures have been given (Jones, 2011; Wang *et al*., 2015; Xu Y *et al*., 2015). Wang (2016a) proved that FDA has better performance in parameter estimation as well as moving target detection, indicating that FDA can be exploited for radar applications (Wang, 2015). FDA was also used to suppress the multipath and range-dependent clutter (Wu *et al*., 2012; Cetintepe and Demir, 2014). Although much of the literature indicates that FDA can be used for range-dependent jamming (Wang and So, 2014; Wang, 2015), a concrete method for its application has rarely been studied. A method of deceptive jamming suppression based on FDA-MIMO (multiple input, multiple output) was proposed by Xu J *et al*. (2015), and is unique in the literature. However, although Xu J *et al*. (2015) introduced the principle and the performance of jamming suppression via spatial frequency in the transmit-receive domain, a concrete method of extraction is still unknown. A method for using FDA in deceptive jamming suppression for improved performance requires further investigation.

Due to the coupling range and angle peak in the beam former output, a standard FDA cannot estimate the range and angle of a target by itself (Wang, 2016b). Traditional phase-array radar (PAR) can estimate the angle information accurately by itself, but not the range information. When the advantages of PAR are used by FDA, physical range information can be correctly extracted under deceptive jamming. In this study, FDA is combined with PAR to distinguish the true target and FTGs; FDA transmits double pulses so that both the range and angle information can be estimated accurately. The strategy is based on the observation that jamming can deceive only the radar in range domains, which is the general situation in ECMs.

2 Preliminaries of frequency diverse array radar

Different from traditional phased arrays, FDA uses a small frequency increment across the elements. Considering that the FDA radar is composed of omnidirectional elements, the carrier frequency of the nth element in a uniform linear form is (Antonik *et al*., 2006)

$$f_n = f_0 + (n-1)\Delta f, \quad n = 1, 2, ..., N, \tag{1}$$

where f_0 is the reference carrier frequency and Δf is the frequency increment, which can be neglected when compared to f_0 (in other words, Δf should meet the condition that $f_0 >> N \cdot \Delta f$).

Supposing that all the signals transmitted by elements have the same initial phase, the signal arriving at a given far-field point (R, θ) (denoting the range and angle for the reference element) is

$$s_n\left(t - \frac{r_n}{c}\right) = \exp\left[\mathrm{j}2\pi f_n\left(t - \frac{r_n}{c}\right)\right], \tag{2}$$

with c denoting the speed of light and $r_n = R - nd\sin\theta$ the distance between the target and the nth element. Therefore, the phase difference of the signals transmitted by different elements can be expressed as (Antonik *et al*., 2006)

$$\Delta\psi(t) \approx 2\pi\left(\Delta f \cdot t + \frac{f_0 \cdot d \cdot \sin\theta}{c} - \frac{\Delta f \cdot R}{c}\right), \tag{3}$$

where d is the inter-element spacing. In a narrowband case, the array factor can be expressed as (Wang, 2016a)

$$\begin{aligned} \mathrm{AF}(t; R, \theta) &= \sum_{n=0}^{N-1} \frac{1}{r_n} \exp\left\{\mathrm{j}2\pi f_n\left[t - \frac{R}{c} + \frac{nd\sin\theta}{c}\right]\right\} \\ &\approx \frac{\exp(\mathrm{j}\phi_0)}{r} \cdot \frac{\sin\left[N\pi\left(\Delta f \cdot t - \frac{\Delta f \cdot R}{c} + \frac{df_0\sin\theta}{c}\right)\right]}{\sin\left[\pi\left(\Delta f \cdot t - \frac{\Delta f \cdot R}{c} + \frac{df_0\sin\theta}{c}\right)\right]}. \end{aligned} \tag{4}$$

The additional phase factor ϕ_0 is

$$\phi_0 \approx 2\pi f_0\left(t - \frac{R_0}{c}\right) - \pi(N-1)\frac{f_0 d\sin\theta}{c}. \tag{5}$$

As shown in Eq. (4), the characteristics of the pattern, all of which are useful for FTG discrimination, can be identified as follows:

1. The beam pattern is range-angle-dependent. For a given instant of time, the angle on which the beam focuses is changed with an increasing range. For a given time, the angle on which the pattern focuses in $R' = R_0 + \Delta R$ can be written as

$$\theta' = \arcsin\left(\sin\theta_0 + \frac{\Delta f \Delta R}{df_0}\right), \tag{6}$$

where θ_0 denotes the angle of the peaks at $R=R_0$.

2. The beam pattern is time-variant. For a fixed range, the pattern would be periodic in time in the angle dimension, and the angle of the peaks at $t=t_0$ can be expressed as

$$\theta' = \arcsin\left(\sin\hat{\theta} - \frac{\Delta f \cdot t_0 \cdot c}{df_0}\right), \tag{7}$$

where $\hat{\theta}$ denotes the angle of the peaks at $t=0$. The tendency of angle changing with increasing time is shown in Fig. 1.

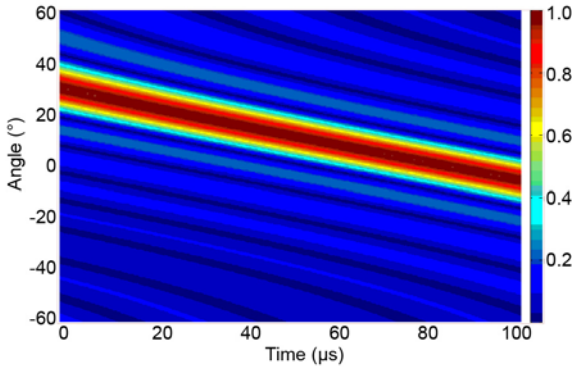

Fig. 1 Angle-time pattern of FDA (Δf=3 kHz, f_0=1 GHz)

3. The beam pattern of FDA has a range resolution (for a transmitted monochromatic continuous-wave signal, conventional PAR has no range resolution). The range modulation patterns of PAR and FDA are shown in Fig. 2, with the energy attenuation in the range dimension being neglected.

4. When the frequency increment is zero, the array factor of FDA will be the same as the array factor of PAR. The patterns of PAR and the FDA are shown in Fig. 3.

The beam can be formed through phase-shift architectures in PAR, which can also be suitable for FDA. Supposing that the phase shift for each element is 0, φ, …, $(N-1)\varphi$, the transmitting patterns of FDA based on Eq. (4) can be written as

$$\left|\mathrm{AF}_{\mathrm{FDA}}\right| = \frac{\sin\left[N\pi\left(\Delta f \cdot t - \frac{\Delta f \cdot R}{c} + \frac{df_0 \sin\theta}{c}\right) - \frac{N\varphi}{2}\right]}{\sin\left[\pi\left(\Delta f \cdot t - \frac{\Delta f \cdot R}{c} + \frac{df_0 \sin\theta}{c}\right) - \frac{N\varphi}{2}\right]}. \tag{8}$$

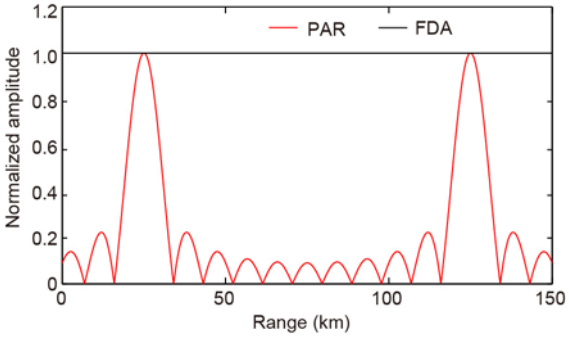

Fig. 2 The modulation patterns of range (θ and t are fixed)

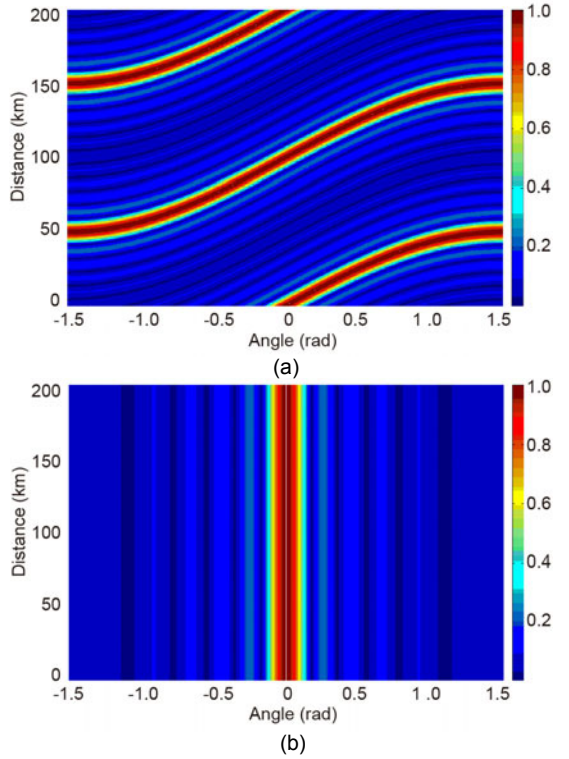

Fig. 3 Comparison of FDA (a) and PAR (b) beam patterns (Δf=3 kHz, f_0=1 GHz)

When the desired position is (R_0, θ_0), the amount of phase shift in $t=0$ should be set as

$$\varphi = 2\pi\left(-\frac{\Delta f \cdot R_0}{c} + \frac{df_0 \sin\theta_0}{c}\right). \tag{9}$$

3 Principle of deceptive jamming discrimination

FTGs are always created by digital radio frequency memory (DRFM) through listening, storing,

and repeating the radar's transmitted signals. PAR can be easily deceived in the range dimension because the range information is extracted by time delay. In the angle dimension, however, the information is extracted through the sum-difference beam and the measurement results can be accurate. Because the range and angle are coupled in FDA, the physical range can be correctly estimated when the angle information of RTG can be obtained. Two strategies are investigated to identify RTG from FTGs in the following, one of which is based on angle comparison and the other is based on range estimation.

3.1 Strategy based on angle comparison (strategy A)

Angle measurement is conducted by a sum-difference amplitude comparison in PAR. Supposing that the target is illuminated by two beams, the echo received by beam 1 is

$$u_1 = kF_1(\theta) = kF(\theta_0 - \delta), \tag{10}$$

while the echo received by beam 2 is

$$u_2 = kF_2(\theta) = kF(\theta_0 + \delta), \tag{11}$$

with θ_0 denoting the angle of the antenna axis and δ the drift angle between two beams and the antenna axis. When the drift angle of the target is ε, the sum and difference signals can be expressed as

$$\begin{cases} \sum(\theta) = u_1(\theta) + u_2(\theta) \approx 2kF(\theta_0), \\ \Delta(\theta) = u_1(\theta) - u_2(\theta) \approx 2k\varepsilon \dfrac{dF(\theta)}{d\theta}\Big|_{\theta=\theta_0}. \end{cases} \tag{12}$$

As shown in Eq. (12), the value of angular error ε is proportional to $\Delta(\theta)$ and the direction of deviation can be indicated by the symbol of sum-difference comparison.

Because the range and angle are coupled, an error will occur in angle measurement when the range under test is not equal to the real range in FDA. Thus, FTGs can be identified due to the mismatch between the test angle and physical angle. Assume that an RTG locating at (R_i, θ_0) and an FTG locating at (R_f, θ_0) are indicated by PAR at the same time. Adjusting by Eq. (9) the beam pattern of FDA to focus on (R_i, θ_0) when t_1=0, another peak would occur when t_2=(R_f−R_i)/c. The angular error ε would be zero when t_1=0, while ε would be nonzero at t_2, according to Eqs. (6) and (7). The angle patterns focused on at (R_i, t_2) and (R_f, t_2) can be given as

$$\begin{cases} \theta_2 = \arcsin\left(\sin\theta_0 - \dfrac{\Delta f \cdot t_2 \cdot c}{df_0}\right), \\ \theta_3 = \arcsin\left[\sin\theta_0 + \dfrac{\Delta f(R_\mathrm{f} - R_t)}{df_0} - \dfrac{\Delta f \cdot t_2 \cdot c}{df_0}\right] = \theta_0, \end{cases} \tag{13}$$

where θ_2 denotes the angle at (R_i, t_2) and θ_3 the angle at (R_f, t_2). Eq. (13) reveals that the pattern steers at θ_0 at (R_f, t_2); at this time, the angular error ε=θ_2−θ_0, so the testing result of the angle is θ_2 at range R_f. That is to say, the angle information cannot be extracted accurately when the range cannot be measured correctly. However, when the physical angle is known to FDA, FTGs will be identified due to angle mismatch.

3.2 Strategy based on range estimation (strategy B)

As shown in Fig. 2, FDA has a range resolution that can be similar to the angle dimension of PAR. Thus, a high-accuracy measurement can also be conducted through the sum-difference beam in the range dimension. This can provide another effective way to estimate the slant range of the target when the echo is deceived in the time domain. When the sum-difference beam is adopted, the target will be illuminated by two beams, which can be expressed as

$$\begin{cases} u_1 = kF_1(R) = kF(R_0 - \delta_R), \\ u_2 = kF_2(R) = kF(R_0 + \delta_R), \end{cases} \tag{14}$$

with R_0 denoting the range of the antenna axis when the angle is fixed and δ_R the drift distance between the two beams and the antenna axis. When the drift distance of the target is ε_R, the sum and difference signals are

$$\begin{cases} \sum(R) = u_1(R) + u_2(R) \approx 2kF(R_0), \\ \Delta(R) = u_1(R) - u_2(R) \approx 2k\varepsilon_R \dfrac{\mathrm{d}F(R)}{\mathrm{d}R}\Big|_{R=R_0}. \end{cases} \tag{15}$$

As stated in Eq. (15), the value and direction of range error ε_R can also be indicated by the signal of sum-difference comparison, which can be the same as

the condition for the angle dimension. In addition, the beam pattern is time-variant based on Eq. (4), and when the angle is fixed, the distance on which the beam focuses at $t=t_1+\Delta t$ can be calculated as

$$R = R_0 + c\Delta t, \tag{16}$$

where R_0 denotes the distance that the radar steers at $t=t_1$. Thus, the beam can scan a distance interval for a given angle without any adjustment, assuming that two targets located at (R_i, θ_0) and (R_f, θ_0) are indicated by PAR at the same time. Steering the beam to (R_i, θ_0) when $t=0$, if the value of the difference signal is zero, then we can conclude that R_i is a physical distance.

3.3 Strategies to transmit double pulses

According to the above analysis, deceptive jamming can be identified successfully in FDA when the information about a real angle can be obtained. An important issue is how to extract real angle information accurately for FDA. One effective way is to emit double coherent pulses with zero and nonzero frequency increments. Double pulses can be transmitted by the same hardware equipment via time sharing and spatial sharing.

The strategy of emitting double pulses via time sharing is illustrated in Fig. 4. All the intrinsic signals are produced by the same local oscillator, which enables better performance in signal coherence. When the radar wants to emit the conventional waveform, switch B is turned on and all elements will emit the same signal. A frequency increment will be brought to every element via a frequency multiplier when switch A is turned on. The phase difference error between elements can be eliminated through amplitude-phase compensation.

The strategy of emitting double pulses can also be conducted via spatial sharing (Wang and Shao, 2012; Wang, 2013), which is shown in Fig. 5. The array will be divided into two subarrays, one transmitting the PAR waveform (subarray 1) and the other transmitting the FDA waveform (subarray 2). Orthogonality of the transmitted waveforms is a requirement for allowing signal separation at the receiver, which can be written as

$$\int S_{\mathrm{P}}(t)\cdot s_n(t)\mathrm{d}t = 0, \quad n=1,2,...,N, \tag{17}$$

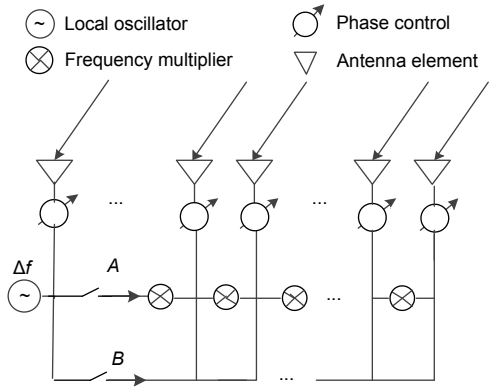

Fig. 4 Illustration of the double-pulse FDA via time sharing

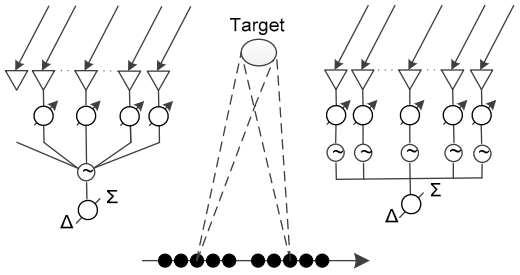

Fig. 5 Illustration of the double-pulse FDA via spatial sharing

where $S_{\mathrm{P}}(t)$ denotes the signal emitted by PAR and $s_n(t)$ the signal emitted by the nth element in subarray 2. The physical angle will be accurately measured in subarray 1, and a new coupling of angles at different distances will be obtained in subarray 2. The physical distance will then be identified when the test results in subarray 2 are compared to those in subarray 1.

Finally, the proposed deceptive-jamming discrimination method (Fig. 6) can be summarized as follows:

1. The FDA radar transmits a coherent pulse with zero frequency increment (Δf=0 Hz).

2. The FDA radar return is processed by the sum-difference comparator and thus the angles of the targets θ_0 can be estimated using Eq. (12).

3. Record the time when the peaks are outputted and thus the ranges of the targets can be estimated.

4. The FDA radar focuses the transmit beam pattern toward the desired position (R_0, θ_0) by Eq. (9) and transmits another pulse with a non-zero frequency increment. R_0 can be the nearest range between the targets and radar, which is indicated and recorded in step 3.

5. For strategy A, record the time when the value of the difference signal in the angle dimension is zero, which can be written as Δt.

6. For strategy B, record the time when the value of the difference signal in the range dimension is zero, which can also be written as Δt.

7. The range of RTG can be estimated as $R=R_0+c\Delta t$.

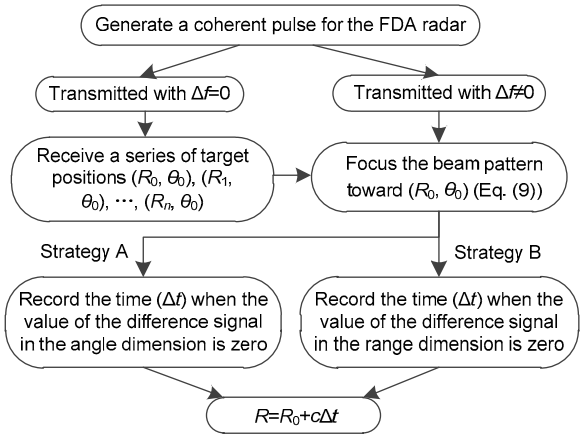

Fig. 6 Diagram for the proposed deceptive-jamming discrimination method

4 Localization performance of the double-pulse strategy

Although the proposed double-pulse strategy can suppress deceptive jamming, it also causes loss in reflected signal energy and decrease in localization performance. In this section, the Cramer-Rao lower bound (CRLB) and detection probability are presented to show how much the localization performance is degraded using the double-pulse strategy.

According to Wang and Shao (2014) and Stoica and Moses (2005), the CRLB for estimating the target angle and range in FDA can be expressed as

$$\mathrm{CRLB}_{\theta_s}=\left(2\cdot\mathrm{SNR}\cdot k_1^2\sum_{n=0}^{N-1}n^2\right)^{-1}, \tag{18a}$$

$$\mathrm{CRLB}_{r_s}=\frac{k_1^2+k_2^2}{2\cdot\mathrm{SNR}\cdot k_1^2k_3^2\sum_{n=0}^{N-1}n^2}, \tag{18b}$$

where SNR stands for the signal-to-noise ratio, θ_s the angle of the target, and r_s the range of the target, and k_1, k_2, and k_3 can be expressed as

$$k_1=2\pi f_0 d\cos\theta_s/c_0, \tag{19a}$$

$$k_2=2\pi(f_0+\Delta f)d\cos\theta_s/c_0, \tag{19b}$$

$$k_3=2\pi\Delta f/c_0. \tag{19c}$$

The detection probability based on the Neyman-Pearson principle (Wang and Shao, 2014) can be expressed as

$$P_\mathrm{d}=1-F_{\chi^2_{(2)}}\left[\frac{\sigma_\mathrm{n}^2F^{-1}_{\chi^2_{(2)}}(1-P_\mathrm{fa})}{\sigma_\mathrm{s}^2N^4+\sigma_\mathrm{n}^2}\right], \tag{20}$$

where $\chi^2_{(2)}$ is the chi-square distribution with two degrees of freedom, N is the number of receive array elements, and P_fa is the false alarm probability. An approximate expression of Eq. (20) is (Richards, 2005)

$$\begin{cases}P_\mathrm{d}\approx 0.5\cdot\mathrm{erfc}\left(\sqrt{-\ln P_\mathrm{fa}}-\sqrt{\mathrm{SNR}+0.5}\right),\\ \mathrm{erfc}(z)=1-\dfrac{2}{\sqrt{\pi}}\displaystyle\int_0^z\exp(-v^2)\mathrm{d}v.\end{cases} \tag{21}$$

From Eq. (18), we can see that when $\Delta f=0$, $\mathrm{CRLB}_{r_s}\to\infty$; it can be easily understood that conventional PAR has no range resolution. Both Eqs. (18) and (21) show that the localization performance is highly correlated with the signal-to-noise ratio (SNR) in the receiver, so an SNR performance comparison between a double-pulse radar and a typical FDA radar is necessary for localization performance analysis.

For a time-sharing FDA radar, the output SNR during one pulse can be the same as the conventional SNR; however, the coherent processing time would decrease as the time-sharing radar transmits double pulses during one coherent processing cycle. Suppose that the process of pulse integration in a double-pulse radar is non-coherent integration, and that M pulses are integrated during one coherent processing cycle. The resulting SNR after integration can be expressed as (Mahafza and Elsherbeni, 2003; Richards, 2005)

$$\begin{cases}\mathrm{SNR}_\mathrm{res}=\mathrm{SNR}_1\cdot I(M)/L_\mathrm{res}(M),\\ \left[I(M)\right]_\mathrm{dB}=6.79(1+0.235P_\mathrm{d})\left[1+\dfrac{\log(1/P_\mathrm{fa})}{46.6}\right]\\ \qquad\qquad\cdot\log M[1-0.14\log M+0.0183(\log M)^2],\\ L_\mathrm{res}(M)=M/I(M),\end{cases} \tag{22}$$

where $I(M)$ denotes the improvement factor of accumulation and L_{res} the SNR losses during the accumulation. For fixed P_{fa} and P_d, the single-pulse SNR, SNR_1, can be calculated as

$$(SNR_1)_{dB} = 10\log\left[SNR_{res} \cdot L_{res}(M) / I(M)\right]. \quad (23)$$

Suppose that the time when radar emits the conventional waveform can be equal to the time when radar emits the FDA waveform in a double-pulse radar. The number of integrated pulses can be $M/2$. So, the ratio of the SNR for a single pulse between a time-sharing radar (denoted as SNR_{1-ts}) and a typical FDA (denoted as SNR_{1-FDA}) can be expressed as

$$\frac{SNR_{1-ts}}{SNR_{1-FDA}} = \frac{L_{res}(M) / I(M)}{L_{res}(M/2) / I(M/2)}. \quad (24)$$

For a spatial-sharing FDA radar, the coherent processing time can be the same as the conventional processing time; however, the transmitting energy can be decreased as the number of elements transmitting the same waveform decreases, so the output SNR during one pulse can be lower than the conventional SNR. Assuming that the array is divided from the middle, the SNR during one coherent processing cycle can be decreased to half of that of the typical FDA (3 dB lower than the typical SNR). Also, as the aperture area decreases, the angle resolution and range decrease; this is shown in Eq. (18).

According to the above analysis, the localization performance can be influenced by only the loss of SNR in a time-sharing radar, while by the loss of SNR and aperture area in a spatial-sharing radar. So, the localization performance of a time-sharing radar is better than that of a spatial-sharing radar (both time and spatial sharing are divided from the middle). All the simulation results given in the following section are based on a time-sharing radar.

5 Simulation results

Considering an L-band (f_0=1 GHz) FDA radar composed of 11 elements (N=11), the frequency increment is chosen as Δf=1 kHz and the inter-element spacing is 0.15 cm. The radar transmits two beams during angle measurement, the drift angles of which are both 1° (δ=1°).

5.1 Example 1: strategy A

In the first example, a target of interest is supposed to reflect a plane wave that impinges on the array from the direction of $\theta=\pi/6$ rad and the slant range of R=30 km. Several FTGs are generated by the target through deceptive jamming, the indicated distances of which can be 28.5, 29.25, 30.75, and 31.5 km in PAR (the modulation time of deceptive jamming is 5 μs). The beam is steered to (30 km, π/6 rad) according to Eq. (10). The beam pattern of FDA and the positions of FTGs and RTG are shown in Fig. 7, from which we can see that the FTGs are still in the main beam and cannot be easily identified.

Adjust the beam to steer at (28.5 km, π/6 rad) when t=0. The angles on which the beam focuses at different times at R=30 km are shown in Fig. 8, corresponding to Eq. (7). We can see that the beam would focus on $\theta=\pi/6$ at R=30 km when t=5 μs, which is the physical angle of the target.

Fig. 9 shows the normalized amplitudes of the difference signals at different angles. The values of the difference signals at different times can be obtained, as shown in the magnification in Fig. 9. When t=5 μs, the amplitude of the difference signal is zero.

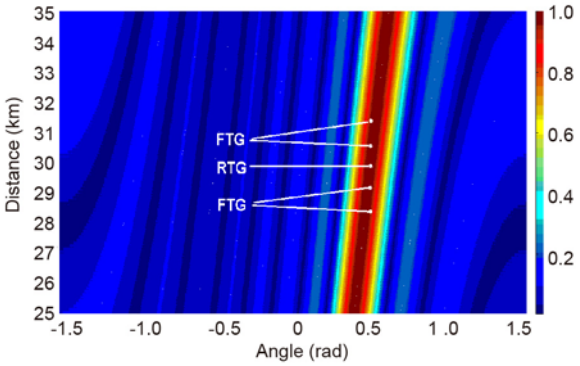

Fig. 7 The beam pattern of FDA and positions of RTG and FTGs

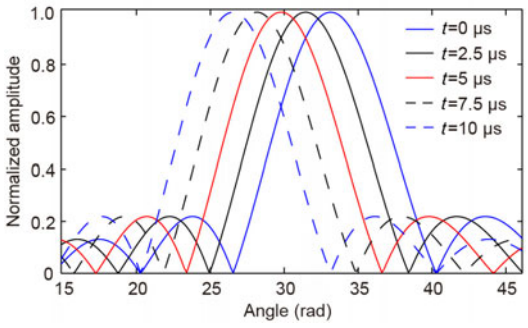

Fig. 8 The beam pattern of FDA at different times

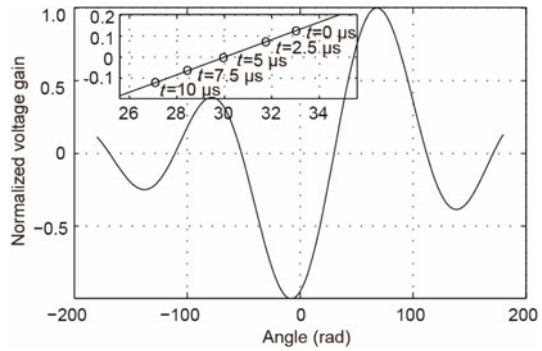

Fig. 9 Normalized amplitude of the difference signal at different angles and times

The testing results of PAR and FDA radar are shown in Fig. 10. We can see that the angle information obtained by these two types of radar can be identical at the physical distance, whereas different at other distances; thus, the RTG can be identified effectively.

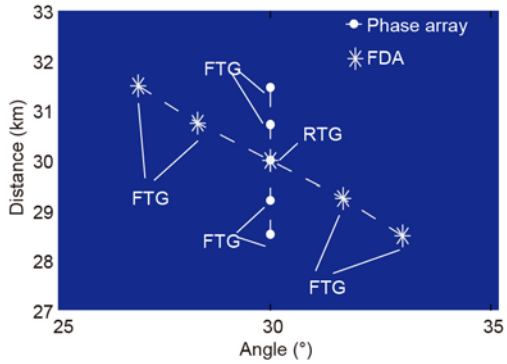

Fig. 10 Testing results of PAR and FDA

5.2 Example 2: strategy B

In this example, the number and location of FTGs can be the same as in Example 1. The radar transmits two beams during range measurement; their slant ranges are 29 km and 31 km at $\theta=\pi/6$ rad. The squinted patterns and sum pattern of the two beams are shown in Fig. 11. The sum pattern focuses on the desired position when the two beams are emitted.

Fig. 12 shows the different patterns of the two beams. Notice that the amplitude of the difference signal has a nearly linear variation with the range when the range error is small enough, which is shown more clearly in the magnification on the left side. Adjusting the sum pattern to focus on (28.5 km, $\pi/6$ rad) when $t=0$, the amplitudes of the difference signal at different times are remarked in the magnification on the right side. When $t=5$ μs, the amplitude of the difference signal is zero and the range can be estimated as $R=R_0+ct=30$ km.

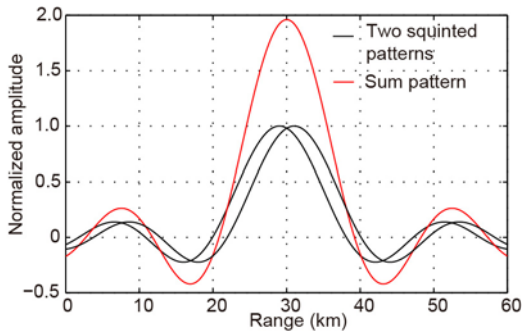

Fig. 11 The squinted patterns and sum pattern of two beams

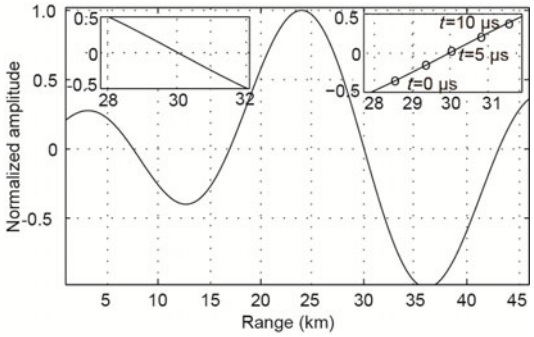

Fig. 12 Normalized amplitude of the difference signal at different angles and times

Fig. 13 demonstrates the difference signal versus N (number of elements) and Δf. We can see that the slope of the difference signal near $R=30$ km has an increasing tendency with growing N or Δf. That is to say, the larger N or Δf is, the better performance can be obtained. So, it can be easily understood that a time-sharing radar has a better localization performance than a spatial-sharing radar because the latter decreases the aperture area.

5.3 Detection and estimation performances

In this example, we simulate the detection and estimation performances of the proposed method. Considering a radar composed of 101 elements, 10 pulses are integrated during one coherent processing cycle. Fig. 14 shows the comparative detection

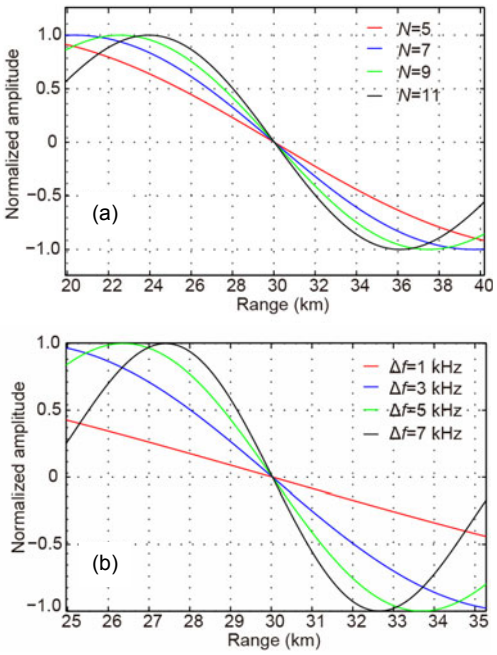

Fig. 13 Normalized amplitude of the difference signal versus N and Δf: (a) difference signal versus N (Δf=3 kHz); (b) difference signal versus Δf (N=11)

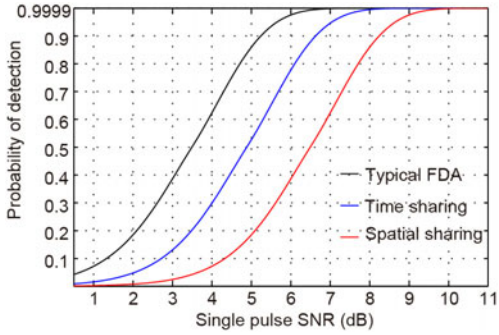

Fig. 14 Comparison of the Neyman-Pearson detection performances

probability as a function of the single-pulse SNR, with a request that $P_{fa}=10^{-8}$. Notice that a double-pulse radar needs a higher single-pulse SNR than a typical FDA radar when the same detection performance is requested. Also, the detection performance of a time-sharing radar can be better than that of a spatial-sharing radar, which is in line with the above analysis.

The localization performance is examined by comparative analysis of the CRLB of the range and angle estimation (Fig. 15). Notice that the localization performance degrades when using the proposed method; however, the performance of a time-sharing radar is close to that of a typical FDA, whereas the spatial-sharing radar is not. When the SNR is large enough, both types of radar can give satisfactory estimation performance.

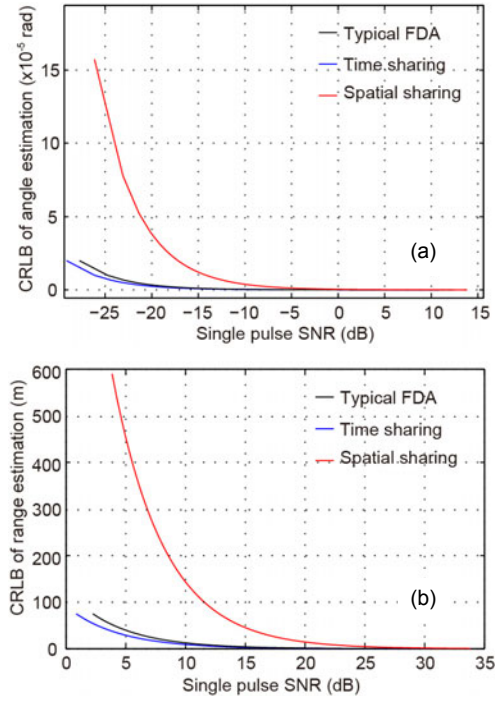

Fig. 15 Target estimation performance versus single-pulse SNR: (a) angle estimation; (b) range estimation

6 Conclusions

FDA radar has drawn much attention in recent years; however, limited work has been conducted on the application of deceptive jamming suppression. Conventional FDA radar cannot estimate the range and angle of a target by itself, whereas PAR can estimate the angle information accurately. In this paper we propose a strategy in which a double pulse can be emitted by FDA so that the advantages of PAR can be used. When the angle information can be extracted by FDA, FTGs can be identified due to the coupling of the range and angle or the resolution in the range dimension. It is also revealed that FDA can offer another way to extract the target range information without time-delay testing, which can provide potential suppression of range-dependent interference.

References

Akhtar, J., 2009. Orthogonal block coded ECCM schemes against repeat radar jammers. *IEEE Trans. Aerosp. Electron. Syst.*, **45**(3):1218-1226. https://doi.org/10.1109/TAES.2009.5259195

Antonik, P., Wicks, M.C., Griffiths, H.D., *et al*., 2006. Multi-mission multi-mode waveform diversity. IEEE Conf. on Radar, p.215-217. https://doi.org/10.1109/RADAR.2006.1631858

Cetintepe, C., Demir, S., 2014. Multipath characteristics of frequency diverse arrays over a ground plane. *IEEE Trans. Antenn. Propag.*, **62**(7):3567-3574. https://doi.org/10.1109/TAP.2014.2316292

Cullens, E.D., Ranzani, L., Vanhille, K.J, *et al*., 2012. Micro-fabricated 130–180 GHz frequency scanning waveguide arrays. *IEEE Trans. Antenn. Propag.*, **60**(8):3647-3653. https://doi.org/10.1109/TAP.2012.2201089

Huang, C., Chen, Z., Duan, R., 2013. Novel discrimination algorithm for deceptive jamming in polarimetric radar. Proc. Int. Conf. on Information Technology and Software Engineering, p.359-365. https://doi.org/10.1007/978-3-642-34528-9_38

Jones, A.M., 2011. Frequency Diverse Array Receiver Architectures. MS Thesis, Wright State University, Dayton, USA.

Lu, G., Tang, B., Gui, G., 2011. Deception ECM signals cancellation processor with joint time-frequency pulse diversity. *IEICE Electron. Expr.*, **8**(19):1608-1613. https://doi.org/10.1587/elex.8.1608

Lu, G., Chen, Y., Lei, Y., *et al*., 2013. Suppression of repeat-intensive false targets based on temporal pulse diversity. *Int. J. Antenn. Propag.*, **2013**:575848. https://doi.org/10.1155/2013/575848

Lu, G., Gui, G., Bu, Y., *et al*., 2016. Deception jammer suppression in fractional Fourier transformation domain with random chirp rate modulation. *J. Chin. Inst. Eng.*, **39**(6): 722-726. https://doi.org/10.1080/02533839.2016.1187081

Mahafza, B.R., Elsherbeni, A.Z., 2003. MATLAB Simulations for Radar Systems Design. Chapman & Hall/CRC, Boca Raton, USA. https://doi.org/10.1201/9780203502556

Rao, B., Zhao, Y.L., Xiao, S.P., *et al*., 2010. Discrimination of exo-atmospheric active decoys using acceleration information. *IET Radar Sonar Navig.*, **4**(4):626-638. https://doi.org/10.1049/iet-rsn.2009.0033

Rao, B., Xiao, S., Wang, X., 2011. Joint tracking and discrimination of exoatmospheric active decoys using nine-dimensional parameter augmented EKF. *Signal Process.*, **91**(10):2247-2258. https://doi.org/10.1016/j.sigpro.2011.04.005

Richards, M.A., 2005. Fundamentals of Radar Signal Processing. McGraw-Hill, New York, USA.

Schuerger, J., Garmatyuk, D., 2009. Performance of random OFDM radar signals in deception jamming scenarios. IEEE Radar Conf., p.1-6. https://doi.org/10.1109/RADAR.2009.4977015

Stoica, P., Moses, R., 2005. Spectral Analysis of Signals. Prentice Hall, Upper Saddle River, USA.

Wang, W.Q., 2013. Phased-MIMO radar with frequency diversity for range-dependent beamforming. *IEEE Sens. J.*, **13**(4):1320-1328. https://doi.org/10.1109/JSEN.2012.2232909

Wang, W.Q., 2015. Frequency diverse array antenna: new opportunities. *IEEE Antenn. Propag. Mag.*, **57**(2):145-152. https://doi.org/10.1109/MAP.2015.2414692

Wang, W.Q., 2016a. Moving-target tracking by cognitive RF stealth radar using frequency diverse array antenna. *IEEE Trans. Geosci. Remote Sens.*, **54**(7):3764-3773. https://doi.org/10.1109/TGRS.2016.2527057

Wang, W.Q., 2016b. Overview of frequency diverse array in radar and navigation applications. *IET Radar Sonar Navig.*, **10**(6):1001-1012. https://doi.org/10.1049/iet-rsn.2015.0464

Wang, W.Q., Shao, H., 2012. A flexible phased-MIMO array antenna with transmit beamforming. *Int. J. Antenn. Propag.*, **2012**:609598. https://doi.org/10.1155/2012/609598

Wang, W.Q., Shao, H., 2014. Range-angle localization of targets by a double-pulse frequency diverse array radar. *IEEE J. Sel. Topics Signal Process.*, **8**(1):106-114. https://doi.org/10.1109/JSTSP.2013.2285528

Wang, W.Q., So, H.C., 2014. Transmit subaperturing for range and angle estimation in frequency diverse array radar. *IEEE Trans. Signal Process.*, **62**(8):2000-2011. https://doi.org/10.1109/TSP.2014.2305638

Wang, Y., Wang, W.Q., Chen, H., *et al*., 2015. Optimal frequency diverse subarray design with Cramér-Rao lower bound minimization. *IEEE Antenn. Wirel. Propag. Lett.*, **14**:1188-1191. https://doi.org/10.1109/LAWP.2015.2396951

Wu, J., Wang, T., Zhang, L., *et al*., 2012. Range-dependent clutter suppression for airborne sidelooking radar using MIMO technique. *IEEE Trans. Aerosp. Electron. Syst.*, **48**(4):3647-3654. https://doi.org/10.1109/TAES.2012.6324751

Xiong, W., Zhang, G., Wen, F., *et al*., 2016. Trilinear decomposition-based spatial-polarization filter method for deception jamming suppression of radar. *IET Radar Sonar Navig.*, **10**(4):765-773. https://doi.org/10.1049/iet-rsn.2015.0348

Xu, J., Liao, G., Zhu, S., *et al*., 2015. Deceptive jamming suppression with frequency diverse MIMO radar. *Signal Process.*, **113**:9-17. https://doi.org/10.1016/j.sigpro.2015.01.014

Xu, Y., Shi, X., Xu, J., *et al*., 2015. Range-angle-dependent beamforming of pulsed frequency diverse array. *IEEE Trans. Antenn. Propag.*, **63**(7):3262-3267. https://doi.org/10.1109/TAP.2015.2423698

Zhang, J., Zhu, D., Zhang, G., 2013. New anti-velocity deception jamming technique using pulses with adaptive initial phases. *IEEE Trans. Aerosp. Electron. Syst*., **49**(2): 1290-1300. https://doi.org/10.1109/TAES.2013.6494414

Zhao, S., Zhang, L., Zhou, Y., *et al.*, 2015. Signal fusion-based algorithms to discriminate between radar targets and deception jamming in distributed multiple-radar architectures. *IEEE Sens. J.*, **15**(11):6697-6706. https://doi.org/10.1109/JSEN.2015.2440769